Cite this paper: Vietnam J. Chem., **2022**, *60(4)*, 417-434 Research article
DOI: 10.1002/vjch.202100166

Corrosion inhibition and adsorption mechanism of *Morus nigra* on mild steel in acidic medium: A sustainable and green approach

Harish Kumar*, Shalu Sharma, Rajni Kumari

Department of Chemistry, Central University of Haryana, Mahendergarh, 123 031, India

Submitted October 30, 2021; Revised December 11, 2021; Accepted December 15, 2021

Abstract

Morus nigra (Mulberry leaves) was tested as a green inhibitor for mild steel (MS) in 0.5 M HCl by theoretical, surface study, and experimental techniques. The impedance, polarization, microscopy, Langmuir, and DFT (computational) techniques were used for the adsorption and corrosion inhibition study. The experimental and theoretical study supports each other results. Adsorption parameters were observed by Langmuir, Gaussian09W (DFT), and BIOVIA Materials Studio Softwares. The surface study was carried out by metallurgical microscopy technique. The theoretical study includes chemical potential, electron-donating power, chemical hardness, HOMO, LUMO, metal inhibitor interaction energy, adsorption energy, etc. UV-visible, NMR, and FTIR studies show that aspartic acid is the major constituent present in the mulberry leaves extract. A 91.62 % corrosion protection was provided by the *Morus nigra* at 1000 ppm. Polarization study proved mixed inhibition. The green inhibitor follows both physical and chemical modes of adsorption. The biochemical and chemical oxygen demand of unused acid left after the gravimetric study was found in an acceptable range.

Keywords. DFT, hydrochloric acid, impedance spectroscopy, mild steel, *Morus nigra*.

1. INTRODUCTION

Metals and their alloys are an important part of the structural unit of different materials used in industry and household equipment. Corrosion is a very serious problem in industry and houses as these metallic parts come to different aggressive environments. Corrosion leads to many types of direct and indirect losses to industry and mankind. The use of synthetic and green corrosion inhibitors in acidic medium is one of the very common methods to prevent corrosion.[1-3] Different organic compounds containing hetero atoms like N, P, S, X, etc., and functional groups composed of heteroatoms acts as a corrosion inhibitor (CI) in the acidic medium.[4,5] Most chemical and organic corrosion inhibitors act by physisorption on the metal by forming an insulating film that minimizes the corrosive attack of inorganic acids.[6-9]

Mild steel (MS) is the main material of construction of trunks, steel almirah, dessert cooler body, wheat grain storer, pipelines, cables, etc. Mild steel possesses unique physical and mechanical properties like mechanical strength, durability, easy availability, and low cost. MS gets easily corroded when got in contact with dilute HCl. Pitting, cracking, and uniform types of corrosion are the common types of corrosion encountered by MS in an acidic environment. Several researchers have tried different chemical and organic corrosion inhibitor (CI) for MS and carbon steel (CS) in acidic medium like miconazole nitrate in HCl medium,[1] natural products (plants and their products),[2] polyamino quinone in HCl medium,[3] antiscalants for industrial cooling water system, TSP for CS, sodium tripolyphosphate (STPP) for CS, *Murraya koenigii* leaves for MS in HCl and H_2SO_4 medium,[4] cyclic and acyclic corrosion inhibitor for CS, plant extract for MS in HCl medium,[5] fruit peel extract for MS in HCl medium,[5] fruit peel extract for CS in HCl,[6] crushed Henna leaves were used for MS in acidic medium,[7] *Carica papaya* as green CI for MS in acidic medium,[8] *Phyllanthus amarcus* for MS in acid medium,[9] lupin for steel in acidic medium,[10] *N. F. wurmb* for MS in HCl medium,[11] coffee ground extract for CS in hydrochloric acid medium,[12] caffeine for CS in alcoholic solution,[13] curry leaves for CS in hydrochloric acid medium,[14] chitosan for MS in HCl medium, etc.

Others have investigated the corrosion inhibition efficiency (CIE) of chitosan for MS in hydrochloric acid,[15] glucose-based polymer,[16] Pectin for steel in acid,[17] and chitin for steel in the acid,[18] PVP for CS in the HCl medium,[19] PVP as for CS in salt

solution,[20] PVP for CS in the HCl medium,[21] PVP-Oxime for MS in the H_2SO_4 medium.[22] Libya-based *Morus nigra* L. was investigated as CI for MS in 1.0 M HCl and a maximum of 94.9 % CIE was achieved at 10 % plant extract.[23] Black Mulberry leaves extract was investigated as CI for the aluminum metal in 2 M HCl solution and shows a 93 % CIE at 2000 ppm of plant extract.[24] Gingko leaves were tested as CI for X-70 steel and shows 90 % CIE at 200 ppm of leaves extract in 1 M HCl solution.[25] H Li *et al.* have proposed reduced graphene oxide and MOF-based epoxy coating for the protection of metals from corrosion.[26] The drug Lasartan potassium was tested as green CI for Q-235 steel and shows 92 % CIE at concentration of 5 mM in dilute HCl solution.[27] Guava leaves extract was tried as green CI for MS in dilute hydrochloric acid by different electroanalytical techniques.[28] *G. indica* was reported as green CI for MS in hydrochloric acid and shows 93 and 87 % CIE in 0.5 M and 1.0 M HCl at 303 K and 80 % CIE in 1.0 M HCl at 333 K temperature.[29] From the literature study, it was observed that a detailed study regarding corrosion inhibition and adsorption mechanism shown by green CI is still lacking by computational, experimental, and surface study techniques for designing new acid organic CI for different metals and their alloys. Black mulberry is a perennial shrub and has lived for many years. It is cultivated throughout the world and is available in plentiful in India in all four seasons. *Morus nigra* L. leaves contain alkaloids, terpenoids, flavonoids, phenolic compounds, etc. which can act as potential green corrosion inhibitors for MS in acidic medium. A detailed study is required on corrosion and adsorption mechanism provided by the green CI by theoretical (DFT, and Langmuir) and experimental techniques.

An extension to previous studies i.e., 5-Aminotetrazole for MS in sulphuric acid,[30] *Murraya K. L.* for MS in HCl,[31] CHA (cyclohexylamine) for MS in sulphuric acid,[32] etc. First and foremost, we are providing the adsorption and corrosion inhibition mechanism of *Morus nigra* in 0.5 M HCl by experimental, computational, and surface study techniques. Impedance, polarization, gravimetric, microscopy techniques were used. Theoretical studies like Density Functional Theory, Frontier MO, MD simulation, Frumkin, and Langmuir Adsorption Isotherm (FAI and LAI) studies were carried out. The waste acid left after the gravimetric study was investigated for its BOD and COD values.

2. MATERIALS AND METHODS

2.1. Material used

MS (IS2062 Fe-350) was used in all the corrosion studies. Table 1 depicts the composition of MS. Polishing of MS specimens was carried out with emery papers of different grades starting from 100 and ending to 600 µm. HCl (CAS number: 7647-01-0, 37 % pure, ACS reagent) was purchased from Sigma Aldrich, Mumbai. Fresh Mulberry green leaves were collected from the CUH campus. They are first dried in open sunlight for continuous two days. Then 10 g of dried powder was dissolved in 100 ml H_2O and boiled until 1/3rd of its volume. Then extract was cooled and make to 100 ml by adding distilled water. This extract was now termed as a stock solution. Further, the concentration of inhibitor was prepared from this stock solution.

Table 1: Percentage composition of Mild Steel

Element	C	Si	Mn	S	P	Ni	Cu	Cr	Fe
Weight % age (w/w)	1.81	0.19	0.72	0.035	0.02	0.3	0.01	0.17	Rest

2.2. Methods

For the gravimetric study, 0.5 M HCl solution was prepared using ultra-pure water with the conductivity of 46 mS/cm. 100, 200, 400, 600, 800, and 1000 ppm of green inhibitor extract was prepared to form a stock solution. The pre-weighed mechanically polished samples of MS were treated with 0.5 M hydrochloric acid in the presence of GCI for 24 h. The American Standard Testing Method (ASTM-D2688) was employed for finding corrosion rate (CR) and inhibition efficiency (IE%).[33] Gravimetric experiments were repeated three times to check the accuracy and precision of the results. The polarization (anodic and cathodic) of the mild steel working electrode was carried out by the PGSTAT-128N (potentiostat/galvanostat). Tafel slopes, $i_{corr,}$ and CR were observed with Nova 1.11 software supplied with the instrument. The electrode potential was measured in reference to the silver/silver chloride electrode. The ASTM (G61) was used for the Tafel plots.[34,35] The potential was scanned from Open Circuit Potential (OCP) to 210 mV in the cathodic direction and OCP to 450 mV in the anodic polarization. A scanning rate of 2 mV/s was used in the polarization study. After the

polarization study, impedance study was performed at OCP from 10 kHz to 1 Hz AC frequency. The American standard test method (G106) was employed in the impedance study.[11,36] The structural details of interface between MS electrode and electrolyte was investigated by Randle's equivalent circuit model. The metallurgical microscopy equipped with Meta Plus software was used for the surface study of corroded MS specimens. The porosity (%), length of pores (μm), and coating thickness (μm) were noticed with Meta-plus software. The Langmuir and Freundlich isotherms were used to study the adsorption and thermodynamic parameters.

The theoretical study was done by Gaussian,[30,37] Avogadro,[31,32] and BIOVIA material studio (BMS). The single point energy, geometry optimization, and frequency study were carried out by Avogadro and Gaussian-09W program. BLYP basis sets of aspartic acid (AA) were used.[35-39] MD simulation was carried out on the surface layer of iron atoms. Adsorption study was performed on NVT ensemble was selected for the theoretical study and a step time of 1 fs of simulation period of 200 ps was used.[40]

The interaction energy of MS/AA, $E_{\text{interaction}}$ was determined by Eq. (1):

$$E_{interaction} = E_{Total} - \left(E_{Surf.+H_2O+H^+ +Cl^-} + E_{Inhibitor}\right) \quad (1)$$

The binding energy ($E_{binding}$) was negative of the $E_{\text{interaction}}$, Eq. (2).

$$E_{\text{binding}} = -E_{\text{interaction}} \quad (2)$$

The computational parameters were determined by Koopman's theorem (Eqn. (3-6).[40,41]

Electrochemical potential: $\varkappa = \frac{(I+A)}{2}$ (3)

Hardness, $\eta = \frac{(I-A)}{2}$ (4)

Softness, $\sigma = \frac{1}{\eta} = \frac{2}{(I-A)}$ (5)

Number of electrons shifted,

$$\Delta N = \frac{(\chi_{Fe}-\chi_{Inh})}{2\times(\eta_{Fe}-\eta_{Inh})} \quad (6)$$

The adsorption energy (E_{ad}) was determined by Eq. (7):

The energy of adsorption, $E_{Ad} = \frac{E_{S-x}-(E_S+E_X)}{n}$ (7)

The other computational parameters were determined by Eqs. (8-15).

Electrophilicity, $\omega = \frac{\mu^2}{2\eta}$ (8)

Charge Transfer Max., $\Delta N_{Max.} = \frac{I+A}{2(I-A)}$ (9)

Adsorption energy, $E_{Ad} = \frac{E_{S-x}-(E_S+E_X)}{n}$ (10)

Electron releasing, $\omega^+ = \frac{(I+3A^2)}{16(I-A)}$ (11)

Electron accepting power, $\omega^- = \frac{(3I+A^2)}{(16(I-A)}$ (12)

Work Function, $\Delta\varphi = -\frac{(\phi_{Fe}-\chi_{Inhib})^2}{4(\eta_{Fe}+\eta_{Inhib})}$ (13)

Back-donation energy, $\Delta\varepsilon_{BD} = -\frac{\eta}{4}$ (14)

Proton Affinity,

$$PA = E_{pro} - (E_{non\ pro} + E_{H^+}) \quad (15)$$

2.3. Biochemical study

The acid containing used water after gravimetric (corrosion) study is normally discarded in to sink. It is very big environmental problem. The strict environmental regulation does not allow to through untreated waste acidified water into environment. To check the biocompatibility of ECI, we have tested the biochemical-oxygen-demand (BOD) and chemical-oxygen-demand (COD) of this waste untreated acidified water before discharging in to environment by standard procedure of Central Pollution Control Board (CPCB) of India.[42,43] The hydrochloric acid left after the gravimetric study was diluted to 10 times with water before biochemical experiments.

3. RESULTS AND DISCUSSION

3.1. Spectroscopic characterization

Figure S1 (ESI) shows UV-visible absorption spectra of extract of Mulberry leaves. The two major peaks appear at 202 and 263 nm which may be due to the presence of Aspartic acid as major constituents present in the extract of Mulberry leaves.[44] Figure S2 (ESI) displays FT-IR spectra of extract of Mulberry leaves. The IR frequency appears at 3500-3350 cm^{-1} (N-H stretching), 3600-2500 cm^{-1} (O-H stretching due to acid group), and 1680 cm^{-1} due to C=O stretching of the aspartic acid group present as a major constituent in the extract of Mulberry leaves. Figure S3 (ESI) shows H^1- proton NMR spectra of aspartic acid present as a major constituent in Mulberry leaves extract. A small peak observed at 7.26 ppm was due to traces of $CHCl_3$ present as impurity present in $CDCl_3$ used as a solvent. UV-visible, FTIR, and NMR studies reveal that aspartic acid is present as a major component in the extract of Mulberry leaves.

3.2. Gravimetric study

Table 2 shows the data obtained from a gravimetric study on mild steel in 0.5 M HCl solution at different concentrations of extract of Mulberry leaves. Although the gravimetric study reveals a rough estimate of CR and IE%, this technique is very important in selecting the corroding medium,

temperature, and time of exposure of the study.[45] Results of the gravimetric study were compared with well-established polarization and impedance spectroscopy techniques. To check and accuracy and reproducibility of results, all the gravimetric experiments were performed in triplicate. The absolute and standard deviations were recorded for each measurement. The maximum absolute deviation observed was 0.05 in the case of blank measurement and the maximum standard deviation observed was 0.02. Figure 1 shows CIE at different concentrations of extract of Mulberry leaves. From Table 2 and figure 1, it was noticed that CR declines and CIE upsurges with the concentration of extract of Mulberry leave i.e., 100 to 1000 ppm. The maximum CIE observed at 1000 ppm concentration was 91.62 %.

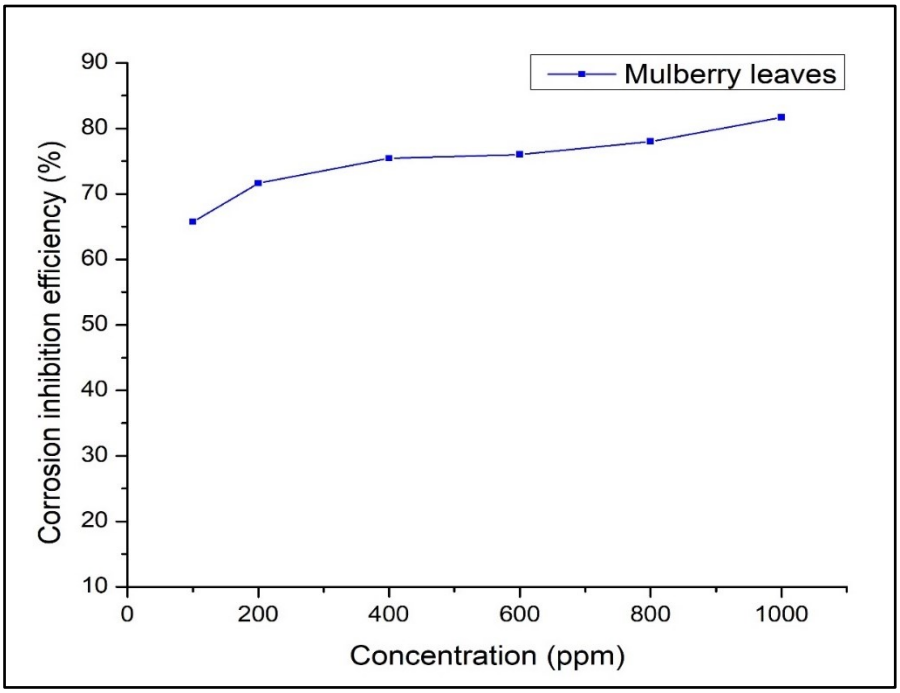

Figure 1: CIE shown by Mulberry leaves extract at different concentration i.e., 200 to 1000 ppm after exposing to 0.5 M HCl for 24 h

Table 2: Corrosion parameters obtained by gravimetric method for Mulberry leaves extract at 25 °C in 0.5 M HCl

Concentration (ppm)	Average weight loss (mg)	Absolute deviation	Standard deviation (σ_d)	Precision in weight measurement	Corrosion rate (mpy)	CIE
Blank	176.2	0.05	0.02	176.2±0.02	716.5	-
100	60.4	0.03	0.01	60.4±0.01	245.46	65.72
200	50	0.04	0.02	50±0.02	203.19	71.63
400	43.3	0.03	0.02	43.3±0.02	175.96	75.43
600	42.3	0.02	0.01	42.3±0.01	171.9	76
800	32.3	0.02	0.01	32.3±0.01	131.26	81.68
1000	14.7	0.02	0.01	32.3±0.02	59.98	91.62

3.3. Polarization study

MS electrode was exposed to 0.5 M HCl solution for approximately 1 h to attain persistent OCP w.r.t. silver/silver chloride electrode. Figure 2 shows a change in OCP w.r.t. time and concentration of green inhibitor. A change in OCP from -520 to -620 mV with the concentration of inhibitor indicates that more and more inhibitor molecules come in the interface region and thus increase the film resistance

and hence increase the OCP value. Figure 3 displays Evans plot for cathodic and anodic polarization of mild steel working electrodes. Table 3 shows electrochemical polarization data of mild steel specimens after exposure to 0.5 M HCl at different concentrations of Mulberry leaves. The i_{corr}. and CR decreases but CIE and resistance polarization (R_p) increase with Mulberry extract concentration in the corrosive medium. The green Mulberry leaves extract shows a minimum of 47.23 % and a maximum of 91.57 % CIE at 100 and 1000 ppm, respectively. The increase in CIE with extract concentration signifies that more and more extract occupies the mild steel/HCl interface region thus forming a barrier film between mild steel and HCl and thus reducing the corrosive attack of HCl on mild steel.[46,47] The increase in CIE with extract concentration also suggests that the breadth of the insulating film upsurges with concentration.

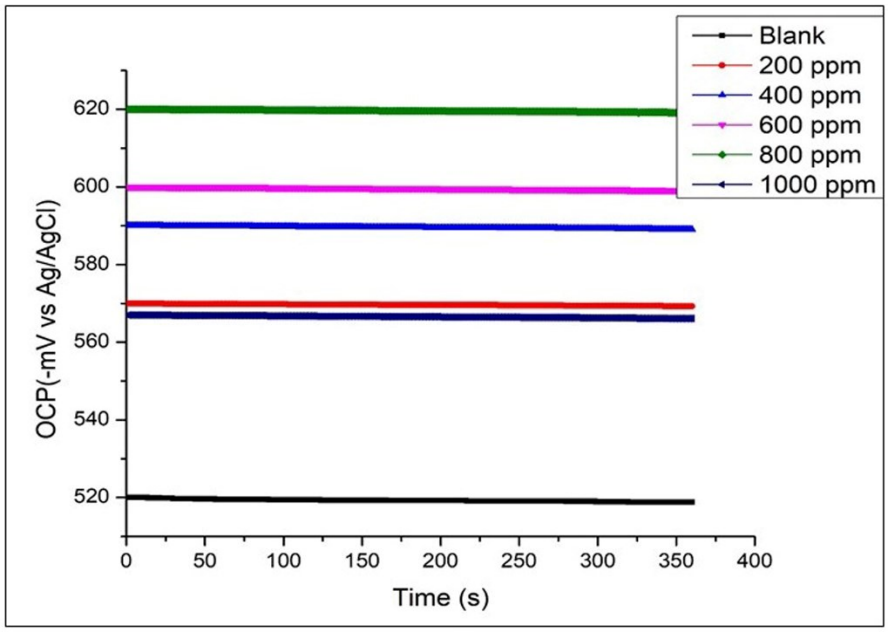

Figure 2: OCP versus time for MS exposed to 0.5 M HCl at different concentration of Mulberry leaves extract

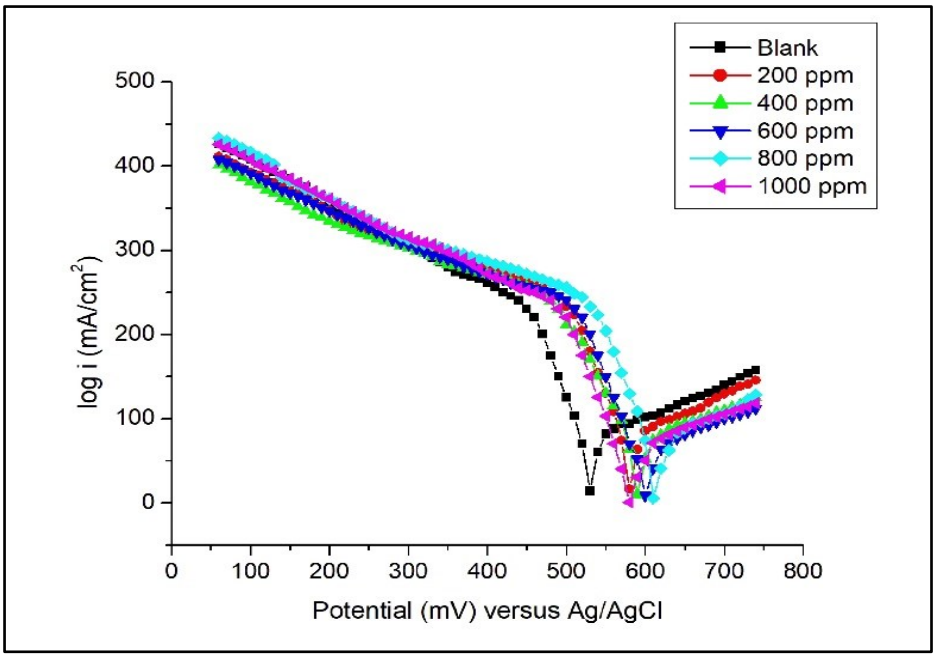

Figure 3: Tafel plots for MS exposed to 0.5 M HCl at different concentrations of Mulberry leaves extract

Table 3: Electrochemical corrosion parameters obtained by polarization technique for Mulberry leaves extract at 25 °C in 0.5 M HCl

Concentration (ppm)	OCP (-mV) w.r.t. Ag/AgCl	I_{corr} (mA/cm^2)	β_a (mV/dec)	$-\beta_c$ (mV/dec)	R_p (Ω/cm^2)	CR (mpy)	CIE (%)
Blank	520	14.48	49.35	32.27	28.7	5.58	-
100	540	6.54	31.34	27.53	31.3	2.52	47.23
200	570	5.28	27.52	22.27	37.4	2.03	53.52
400	590	5.10	21.19	17.43	41.3	1.96	61.27
600	600	4.73	17.14	13.14	47.7	1.82	71.18
800	620	4.51	14.83	11.37	57.8	1.73	78.76
1000	567	1.41	11.35	07.57	61.7	0.47	91.57

3.4. Impedance study

Polarization and gravimetric study were supported by the impedance spectroscopy technique. Impedance spectroscopy is an advanced method to analyze the structure of the metal/inhibitor interface, mechanism of adsorption, and inhibition.[48,49] Impedance technique was performed on the same mild steel working electrode at OCP. The AC frequency was varied from 0.1 to 10,000 Hz and corresponding impedance and phase angle were recorded in the form of Nyquist and Bode plots. Table 4 shows impedance spectroscopy data of mild steel working electrodes. The R_{ct}, R_s, and CIE increase due to the upsurge in width of the electrified interface due to adsorption of a greater number of green inhibitors in the interface region whereas C_{dl} decreases (due to a decrease in dielectric constant in the interface region) with green extract concentration. Mulberry leaves extract shows a minimum of 54.96 % at 200 ppm concentration and a maximum of 90.67 % CIE at 1000 ppm concentration. This increase in IE% with green extract concentration proves an upsurge in film resistance and the same was supported by an increase in R_{ct}. Figure 4 shows the Nyquist plot between real and imaginary impedance. Figure 5 shows a Bode plot between frequency and real impedance for mild steel working electrodes. Figure 6 shows Bode phase shift at different concentrations

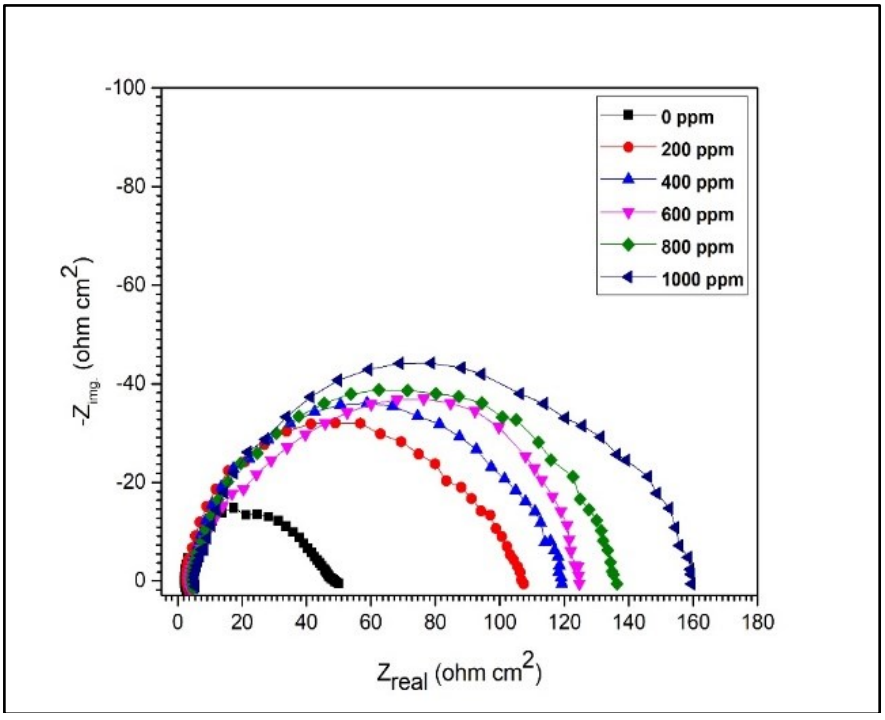

Figure 4: Impedance plots of MS exposed to 0.5 M HCl at different concentrations of Mulberry leaves extract

Table 4: Impedance parameters for MS in 0.5 M HCl at different concentrations of Mulberry leaves extract

Concentration (ppm)	R_s (Ω cm^2)	C_{dl} (× 10^{-3} F cm^2)	R_{ct} (Ω cm^2)	CIE	θ
Blank	2.41	98	2.76	-	-
200	3.54	44.13	4.24	54.96	0.55
400	6.81	39.14	5.62	60.06	0.60
600	7.11	31.43	7.82	67.92	0.68
800	11.45	27.42	14.17	72.02	0.72
1000	15.57	9.14	15.84	90.67	0.91

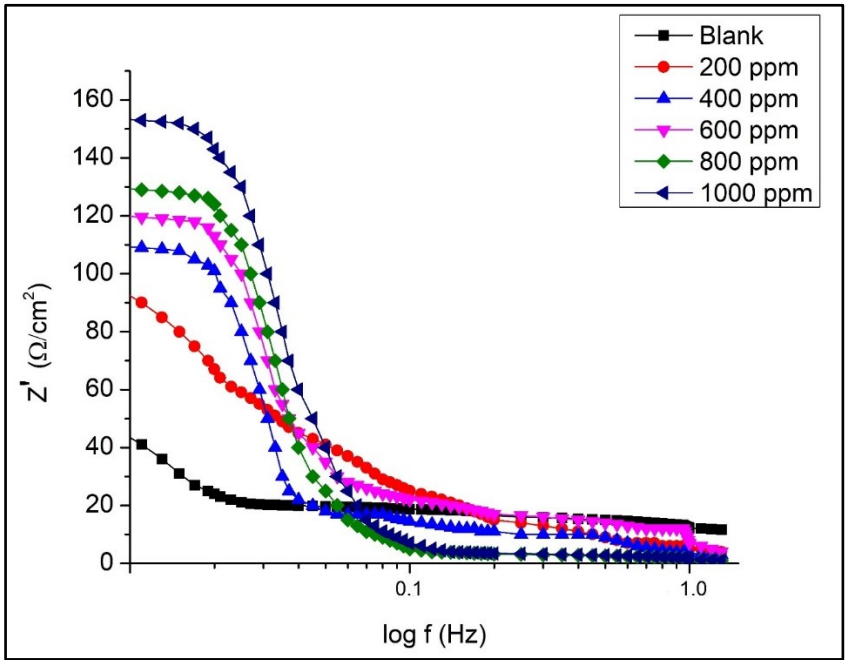

Figure 5: Bode plots of MS exposed to 0.5 M HCl at different concentration of Mulberry leaves extract

of Mulberry leaves extract. Figure 6(B) shows the corresponding Randle equivalent circuit model of MS/HCl interface. From the Nyquist plots, it was observed that the diameter of the semicircle increases with green extract concentration. The R_{ct} increases with an increase in concentration. In general, an increase in the concentration of inhibitor in the interface region increases the heterogeneous character, alters the structure and orientation of dipole, reorientation of charges, surface roughness, and dielectric constant of the medium.[50] The same was happened in our case also supported by an increase in R_{ct}, R_s, and decrease in C_{dl}. The area under the curve (Bode plot, figure 5) upsurges with the concentration of green extract. Hence, CIE upsurges with inhibitor concentration. The Bode phase angle shift from 42 (Blank) to 153 Ω/cm^2 (1000 ppm). The R_{ct} is in parallel with CPE and R_s is in series with CPE. As the value of both R_{ct} and R_s increases with green extract concentration and hence minimizes the corrosion rate.

3.5. Surface study

To study the surface morphology of mild steel specimens after exposure to 0.5 M HCl solution with and without (Blank) Mulberry leaves extract, the metallurgical microscopy (MM) technique was used. The nature of erosion, surface roughness in the form of pores, pits, cracks, and types of corrosion (intergranular, crevice, uniform, etc.) was investigated with the help of the MM technique.[31,32] Figure 7 shows MM images of corroded mild steel specimens after being exposed to 0.5 M HCl solution for 24 h with and without green leaf extract of Mulberry leaves. Table 5 shows the MM surface parameters of mild steel specimens were obtained with the Meta-Plus software. In the blank mild steel specimens, cracks and patches were visible which were created due to corrosive attack of HCl. The

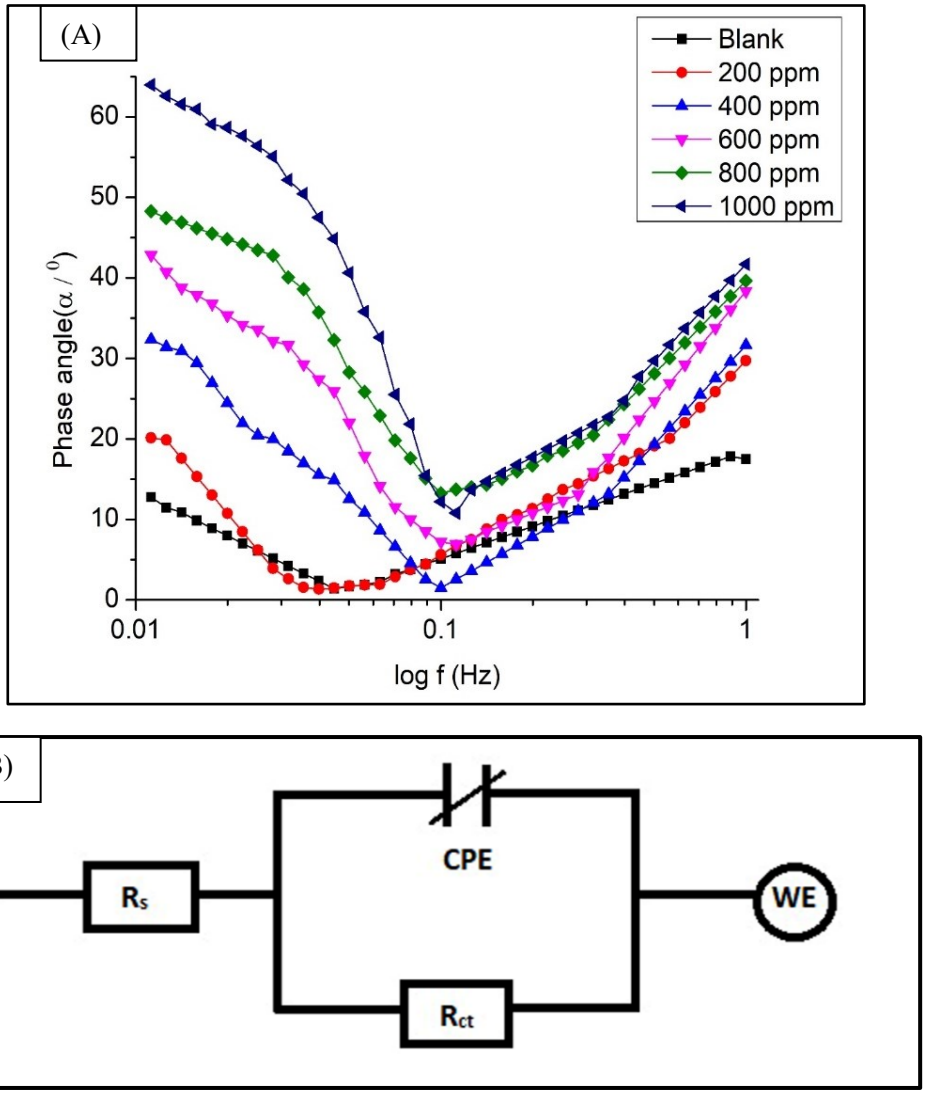

Figure 6: Bode phase angle versus frequency (A) at different concentration of Mulberry leaves extract and Randley equivalent circuit model (B)

Table 5: Surface study parameters of MS at different concentration of Mulberry leaves extract by MM technique

Inhibitor (concentration)	Coating thickness (µm)	Percentage porosity (%age)	Pore length (µm)
Blank	18.64	61.74	45.63
200	23.46	42.46	32.23
400	37.14	31.42	25.76
600	48.63	27.91	21.32
800	61.84	23.7	17.46
1000	83.78	18.14	11.24

intensity of cracks and patches on the surface of MS reduces with Mulberry leaves extract concentration. The coating thickness increases from 18.64 (blank) to a maximum of 83.78 µm (1000 ppm). The percentage porosity decreases from 61.74 % (blank) to a minimum of 18.14 % (1000 ppm) with a green inhibitor concentration. The pore length decreases from 45.63 µm (blank) to a minimum of 11.24 µm (1000 ppm). The surface data shows an upsurge in the breadth of the insulating film with Mulberry leaves extract concentration in the corrosive medium. This is the probable reason for an upsurge in CIE with the concentration of leaf extract. The surface study parameters were supported by impedance spectroscopy data.

3.6. Adsorption study

LAI and FAI study was performed to understand the adsorption mechanism shown by the extract of Mulberry leaves. The two types of adsorption i.e., physical or chemical can take place between the inhibitor and mild steel. The validity of Langmuir

adsorption isotherm proves chemical adsorption and the validity of Freundlich isotherm proves physical adsorption of the green CI molecule on MS surface.[51] The help of experimental data from the impedance and polarization study was taken to find the degree of surface covered by the green inhibitor.

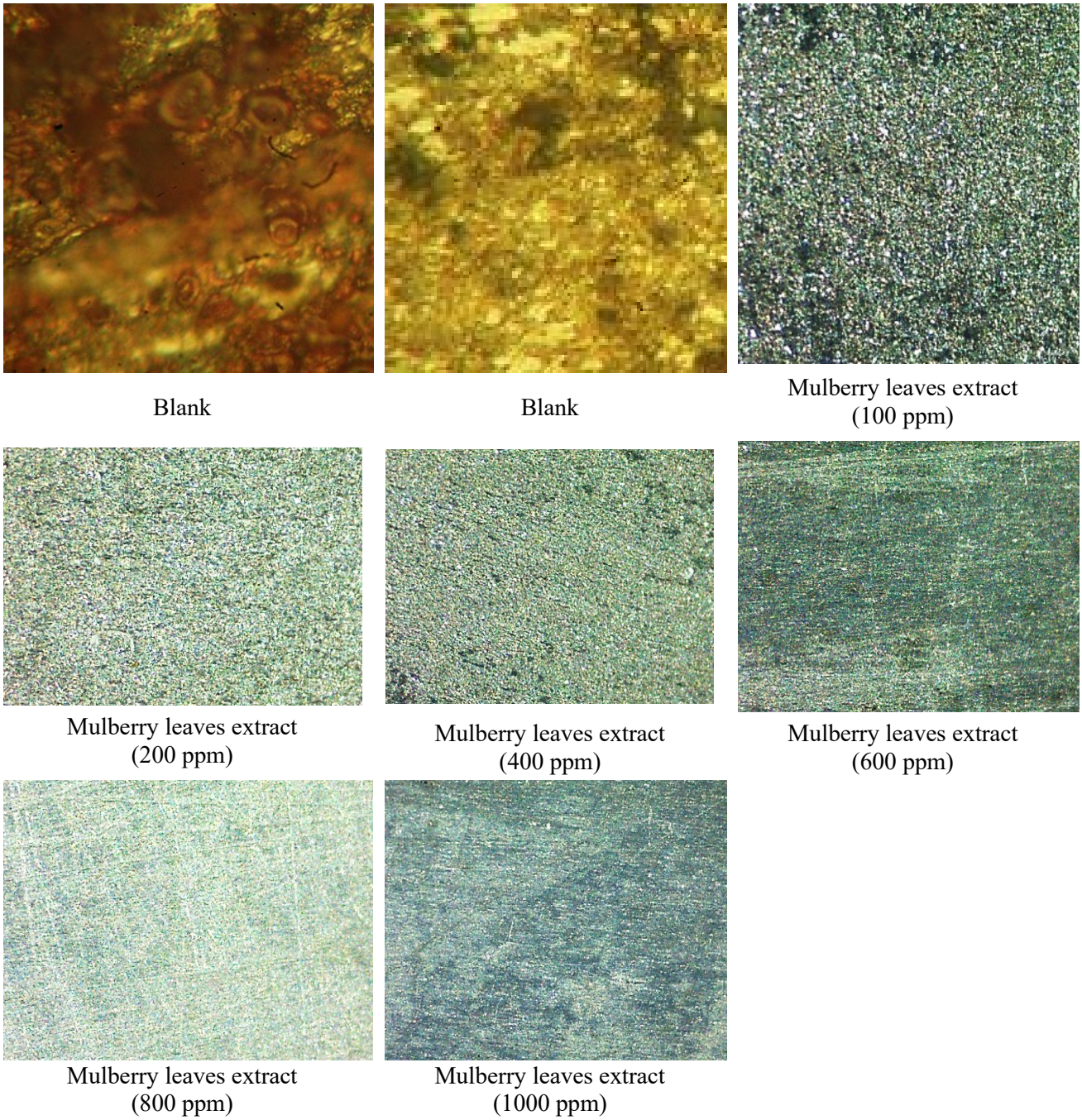

Figure 7: Metallurgical images of MS samples at different concentration of Mulberry leaves extract

The equilibrium constant of adsorption, K_{ads}, the standard free energy involved in adsorption process (ΔG°_{ads}), standard heat of adsorption (ΔH^{0}_{ads}), standard entropy of adsorption (ΔS^{0}_{ads}), and activation energy involved in adsorption were calculated by Eqn. (16-20):

$$\frac{C_{In}}{\theta} = \frac{1}{K_{ads}} + C_{Inh} \quad (16)$$

$$\Delta G^{0}_{Ads} = -RTln(55.5 \times K_{Ads}) \quad (17)$$

$$lnK_{ads} = \frac{-\Delta H^{0}_{ads}}{RT} + \frac{\Delta S^{0}_{ads}}{R} \quad (18)$$

$$\Delta G^{0}_{ads} = \Delta H^{0}_{ads} - T\Delta S^{0}_{ads} \quad (19)$$

$$log\ CR = logA - \frac{E_a}{2.303\ RT} \quad (20)$$

The Langmuir isotherm was plotted between c/θ versus concentration of inhibitor (figure 8) by Eq. (16). Figure 8 shows LAI and FAI for Mulberry leaves extract chemisorbed on the MS. The regression coefficient, R^2 was linear to CI concentration i.e., 0.997 which follows LAI, and confirms monolayer chemical adsorption of Aspartic acid present as major constituents in Mulberry leaves. Table 6 depicts adsorption parameters of Mulberry leaves extract on the MS.

The activation energy is very important in deciding whether adsorption is kinetically or thermodynamically controlled. "If the activation energy is small then interface chemistry is said to be kinetically controlled. If activation energy is large then interface reactions are in thermodynamic control. The chemical adsorption of green inhibitor was possible due to the formation of a stable bond between a heteroatom of inhibitor molecule (N and O atoms) and Fe atoms of mild steel".[51] The chemical adsorption of Mulberry leaves extract tends to increase in ΔS^0_{ads}. The significant free energy of adsorption i.e., -23.46 kJ/mol proves spontaneous and robustness of the adsorption. In contrast, the significant E_a that is 24.4 kJ/mol is disfavoring the spontaneity of the adsorption. Therefore, the adsorption of extract of Mulberry leaves on mild steel surface was kinetically controlled. The $log\frac{\theta}{(1-\theta)} < 1$ (figure 8) signifies the physical adsorption of green inhibitors on mild steel. Hence, from the adsorption study, it is concluded that both types of that are physical and chemical adsorption was possible on the MS surface. The same conclusion was reached by the DFT study.

Table 6: Adsorption parameters (LAI and FAI) for Mulberry leaves extract (1000 ppm) adsorbed on MS in 0.5 M HCl at 25 °C

Temperature (°C)	Slope	R^2	K_{ads} (L/mol)	ΔG^0_{ads} (kJ/mol)	ΔH^0_{ads} (kJ/mol)	ΔS^0_{ads} (kJ/mol. K)	E_a (kJ/mol)
25	1.102	0.997	127.25	–23.46	–26.75	0.011	24.4

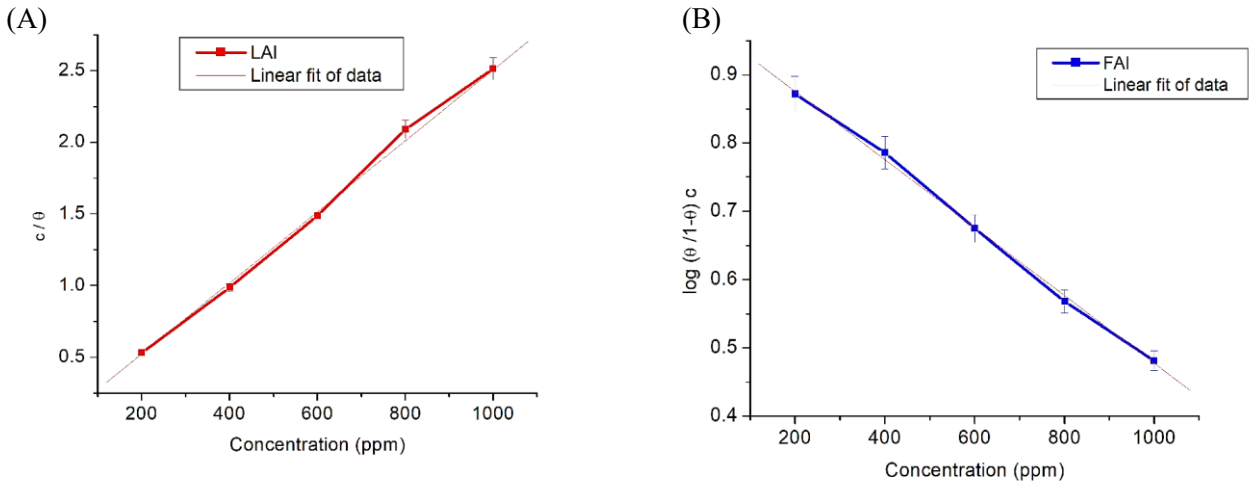

Figure 8: LAI and FAI for Mulberry leaves extract (A) and (B), respectively adsorbed on the surface of MS

3.7. Computational study

The experimental results were supported by the computational study. The DFT study was carried out on the geometry optimized structure of Aspartic acid. The Frontier MO and MD simulation techniques help study adsorption mechanisms and in finding the attacking sites of the inhibitor molecule.[52] Aspartic acid has an almost planar structure and contains two hetero atoms i.e., O and N which contain lone pair of electrons and hence act as a very suitable inhibitor molecule for adsorption of mild steel.

3.7.1. Frontier MO study

The attacking sites of the inhibitor molecule are decided by HOMO and LUMO of the Aspartic acid molecule. Figure 9 represents geometry optimized structure, electron distribution per atom, and van der

Waal surface of Aspartic acid. Fig. 10 depicts the electronic structure, cloud of HOMO, and LUMO of Aspartic acid. Table 8 represents different chemical interaction parameters obtained from the computational study. Table 9 depicts theoretical parameters like a dipole moment, kinetic energy (KE), *E*, heat capacity, *S*, E_{vib}, internal energy, and heat content correction terms, etc.

The Mulliken distribution of charge per atom decides the attacking site of adsorption. Table 7 depicts Fukui's function for radical and attacking sites of Aspartic acid. Higher is the charge on the atoms, greater is the adsorption capacity of that green CI.[53] The electron-donating capacity of inhibitor molecule increase with increase in energy of HOMO. The electron gaining ability of any green CI increases with decrease in energy of LUMO.[54] The HOMO energy of Aspartic acid was significant, and hence it has greater electron-donating capacity.[55] The fraction of electron transferred (ΔN) provides information of transfer of charge from Aspartic acid to MS (table 8).[56] The ΔN of Aspartic acid was found to be significant (table 8), and hence the transfer of charge is from Aspartic acid to mild steel takes place.

The strength of Aspartic acid-MS interaction depends mainly on the extent of electrochemical potential (μ). The μ of Aspartic acid was appreciable and was responsible for high CIE. The high eigenvalue of HOMO of Aspartic acid i.e., 7.71 eV is the main reason for the high corrosion efficiency shown by the inhibitor. A high global softness parameter indicates that Aspartic acid acted as a base and mild steel as an acid. The high energy of interaction further approves the significant adsorption of Aspartic acid.[57]

The electrophilic (LUMO) and nucleophilic (HOMO) active sites of Aspartic acid were shown in Figure 10. The CIE of the inhibitor depends upon magnitude of ΔE_{gap}. The lesser is the ΔE_{gap}, the more is the CIE of inhibitor.[58] In the aspartic acid, nucleophilic sites were present on the terminal COOH group. The electrophilic sites were present on another carboxylic group and its adjoining C atom (figure 10). The electron loving (electrophilic) and nucleus loving (nucleophilic) sites of Aspartic acid prove that inhibitor can adsorb from terminal O atom present adjacent to NH_2 group. The electron releasing tendency of aspartic acid was observed greater than the electron gaining tendency. A strong physical and chemical adsorption of aspartic acid takes place on the mild steel due to the high possibility of back donation.

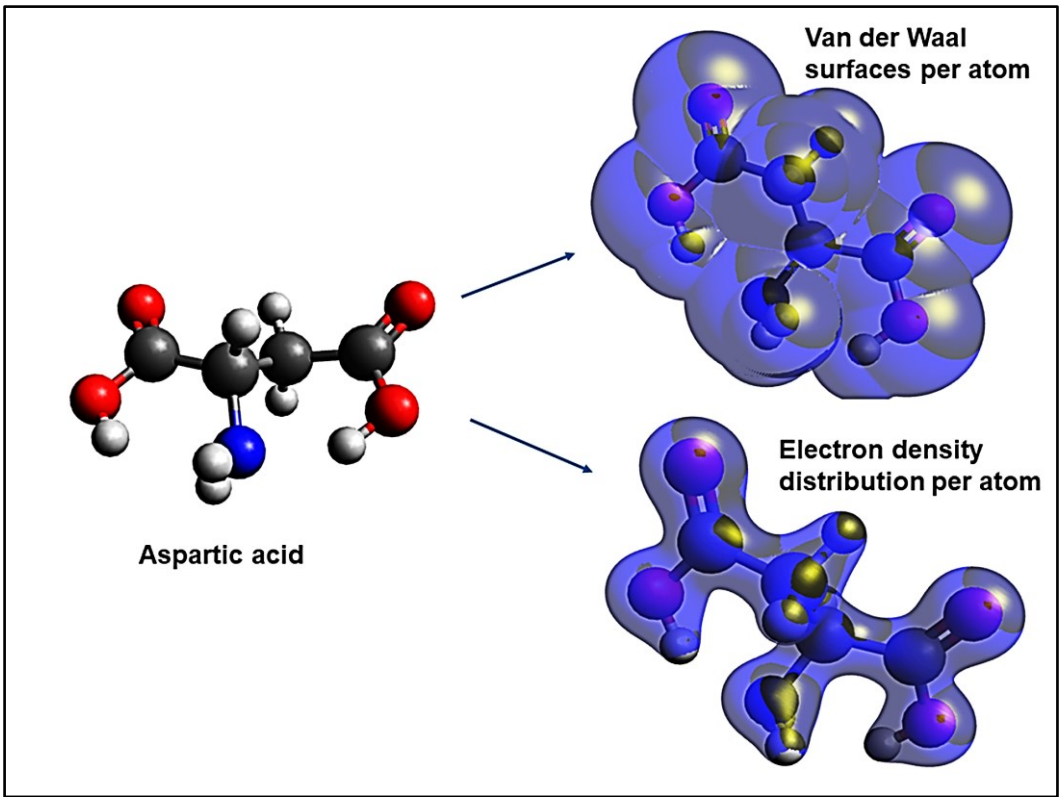

Figure 9: Structure of Aspartic acid, van der Waals surfaces and Electron Density Distribution (EDD) per atom, clockwise

Table 7: Fukui parameters of Mulberry leaves extract for Fe (110) of MS

	Nucleophilic Attack (+)		Electrophilic Attack (-)		Radical Attack (0)	
Atom	Mulliken	Hirshfeld	Mulliken	Hirshfeld	Mulliken	Hirshfeld
C (1)	0.017	0.015	0.122	0.110	0.070	0.063
C (2)	-0.045	0.014	-0.017	0.047	-0.031	0.031
C (3)	-0.052	0.035	-0.009	0.016	-0.030	0.026
N (4)	-0.019	0.036	-0.015	0.014	-0.017	0.025
O (5)	0.062	0.057	0.359	0.365	0.211	0.211
O (6)	0.028	0.033	0.087	0.112	0.058	0.073
C (7)	0.233	0.210	0.026	0.022	0.130	0.116
O (8)	0.214	0.218	0.065	0.062	0.139	0.140
O (9)	0.099	0.124	0.041	0.046	0.070	0.085
H (10)	0.028	0.015	0.052	0.042	0.040	0.029
H (11)	0.067	0.055	0.026	0.020	0.047	0.037
H (12)	0.060	0.024	0.088	0.047	0.074	0.036
H (13)	0.035	0.016	0.057	0.031	0.046	0.024
H (14)	0.146	0.072	0.043	0.019	0.094	0.046
H (15)	0.065	0.036	0.034	0.020	0.050	0.028
H (16)	0.062	0.037	0.041	0.026	0.051	0.031

Table 8: Computational parameters of Aspartic acid for MS in 0.5 M HCl.
(Standard basis set: B3LYP and hybrid functional: 6-31G(d) (6D, 7F)

E_{HUMO} (eV)	E_{LUMO} (–eV)	ΔE (eV)	I (eV)	A (eV)	χ (eV)	η (eV)	σ (eV^{-1})	ΔN (eV)	E_{Ad}(kJ /mol)	ω (au)	ω^+ (au)	ω^-(au)	ΔΨ (-eV)	PA (eV)
7.71	4.07	3.64	7.71	-4.07	1.82	5.89	0.169	0.154	-75.5	3.761	0.304	0.2106	0.567	–0.137

ΔE: Energy gap, I: Ionization energy, A: Electron affinity, χ: Electrochemical potential, η: Hardness, ΔN: Charge transfer parameter, E_{Ad}: Adsorption energy, ω: Electrophilicity, ω^+: Electron accepting tendency, ω^- : Electron donating tendency, ΔΨ: Metal Aspartic acid interaction energy, PA: Proton affinity.

3.7.2. MD Simulation study

Figure 11 shows adsorption locator configurations of aspartic acid on Fe(1 1 0). Table 10 represents adsorption constraints that are $E_{Adsorption}$ (kJ/ mol), $E_{Binding}$ (kcal/mol), and $E_{Interaction}$ (kcal/mol) of aspartic acid. High $E_{Interaction}$ that is -67.65 kcal/mol, and high $E_{Binding}$ and $E_{Adsorption}$ that is 67.65 kcal, and -75.5 kJ, respectively indicates a greater affinity for adsorption of aspartic acid on mild steel. Small E, high S, and μ prove the physio and chemo sorption of aspartic acid on mild steel. A high PA, $\Delta\Psi$, and E_{Ad} further confirms strong physicochemical sorption and high CIE of aspartic acid at a low concentration that is 200 ppm.[58,59] The high dipole moment of 6.65 D was due to the high order of polarity present in aspartic acid (table 9). A low value of rotational constant (B = 3.269 GHz) was due to a high moment of inertia. A high heat capacity i.e., 32.3 $cal.mol^{-1}.K^{-1}$ represents a high order of thermal stability of aspartic acid and hence it can be suitable to adsorb to MS even at high temperatures (table 9). A high value of entropy (S = 94.03 $cal.mol^{-1}.K^{-1}$) signifies that aspartic acid is a stable molecule and has an independent existence in the gaseous phase.

The geometry optimized structure of aspartic acid tells that the adsorption can be from the terminal carboxylic acid group (figures 9 and 10). The vacant 3*d*-orbitals of iron atom (MS) can receive electrons. In reverse, π*- orbitals on the terminal carbonyl group of acid can accept electrons from d-orbitals present at the surface of MS.[59] Nearly flat and straight-chain of aspartic acid molecule adsorb on iron leading to strong barrier film of inhibitor molecules (figure 11).[60,61] The same was reinforced by the high energy of interaction, $E_{binding}$, and $E_{ads.}$ parameters (table 10). Figure 12 shows variation in E_{Total} (Total energy), $E_{Avr.Total}$, VW_{energy} (van der Waals energy), $E_{Electrostat.}$, and $E_{Intramol.}$ (Intramolecular energy) versus

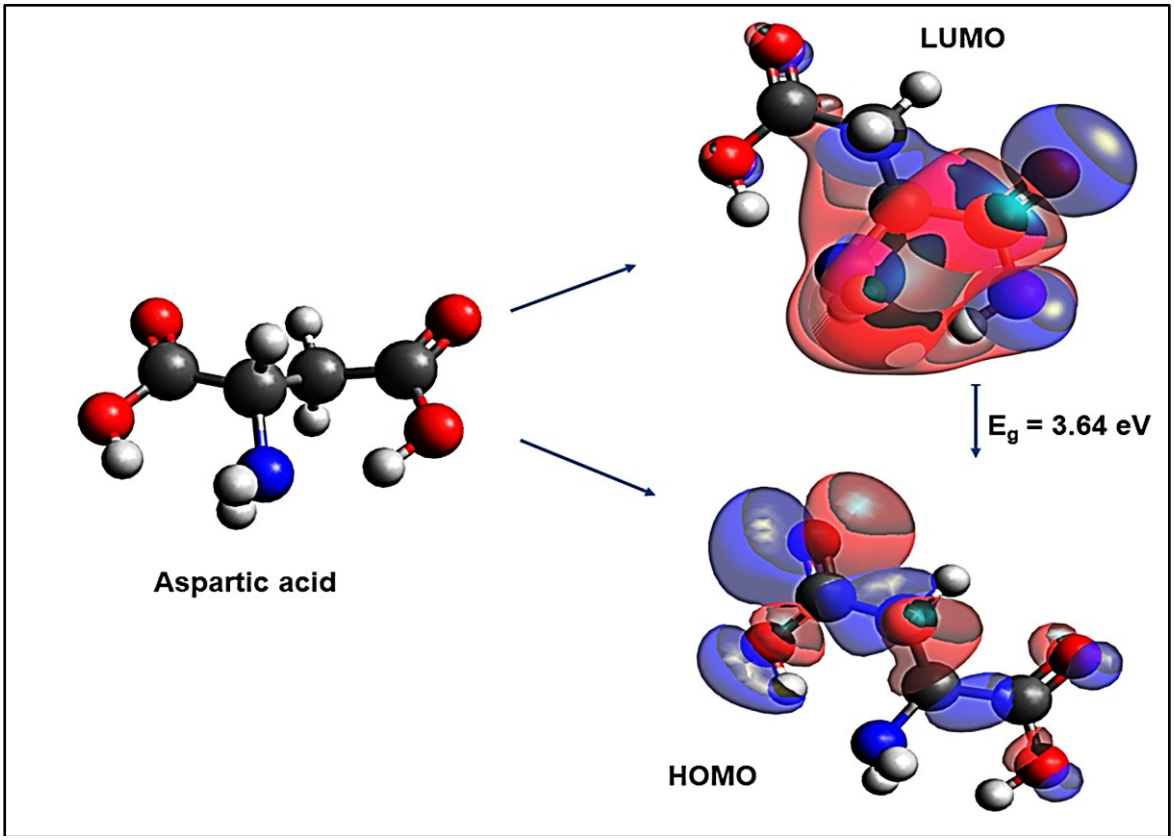

Figure 10: Structure, HOMO and LUMO of Aspartic acid, clockwise

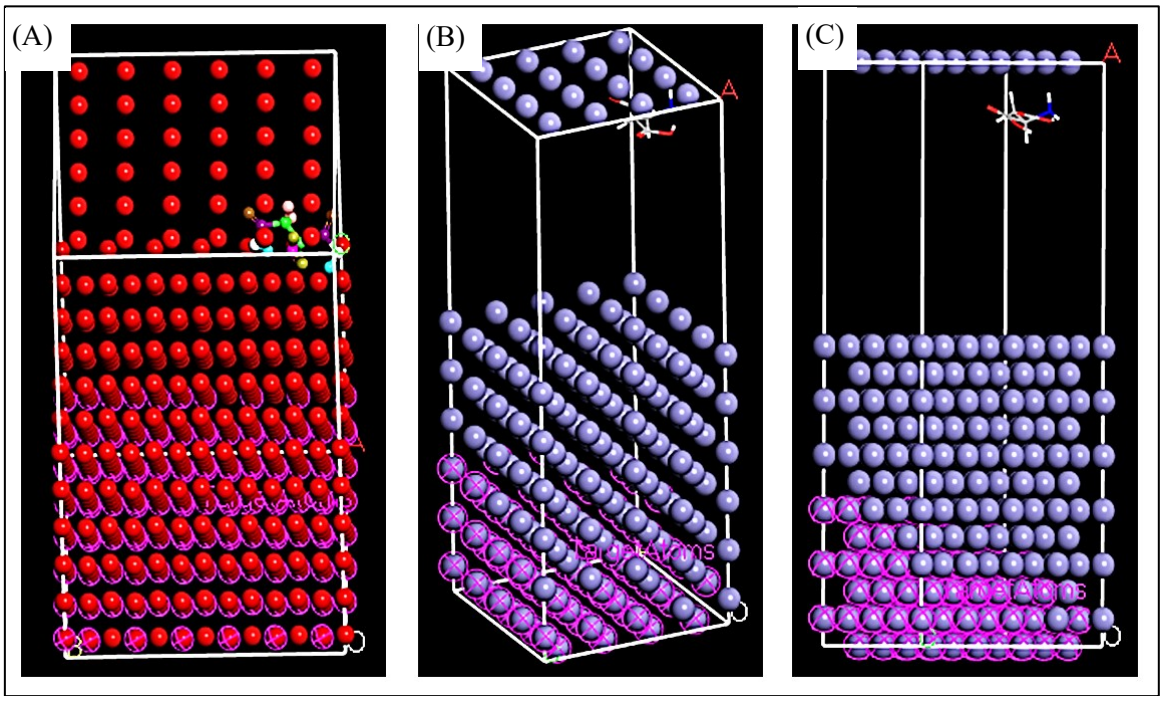

Figure 11: Adsorption study of Aspartic acid on Fe (110) by the adsorption locator module (A): top view, (B and C): side view

optimization steps. Average total energy decreases from -43 kcal/mol to -65 kcal/mol after 50000 optimization steps. Thereafter, it remains almost constant up to 240000 optimization steps. Intramolecular energy remains almost constant i.e., 9 kcal/mol up to 240000 optimization steps.

Electrostatic energy was almost zero even after 240000 optimization steps. It is the van der Waals energy that shows variation up to 20000 optimizations and thereafter becomes constant up to 50000 optimization steps and then again shows variation up to 80000 optimization steps and then again become constant up to 100000 optimization steps and so on.

Table 9: Computational parameters for Aspartic acid ($C_4H_7NO_4$) for MS in 0.5 M HCl. Standard basis: B3LYP and hybrid function: 6-31G(d) (6D, 7F)

Nuclear Repulsive energy (Hartrees)	Rotational constants (GHz)	Dipole moment (D)	Quadrupole moment (xy axis)	KE of Symmetry A'	KE of Symmetry A''	Molecular mass (amu)	Internal Energy, E (Thermal) kCal/mol	Heat capacity, C_V (Cal mol^{-1} K^{-1})	Entropy, S (Cal mol^{-1} K^{-1})	Zero-point vibrational energy (kCal/mol)	Thermal Correction to E (Hartree/Particle)	Thermal correction to Enthalpy, H (Hartree/Particle)	Thermal correction to G (Hartree/Particle)
463.41	3.2698	6.6568	-7.4901	1.047 $\times 10^3$	4.662 $\times 10^1$	133.0375	83.591	32.309	94.038	77.98993	0.133210	0.134155	0.089474

The data reported in table 9 refers to calculations made in gaseous phase.

Table 10: Adsorption parameters obtained from adsorption locator module of Aspartic acid on the Fe (110) atoms of MS

Systems	$E_{interaction}$ (kcal/mol)	$E_{binding}$ (kcal/mol)	Adsorption energy, $-E_{Ads}$ (kJ mol^{-1})
Fe-Aspartic acid	-67.65	67.65	75.5

H_2O molecule = 150, hydrogen ions = 15, chloride ions = 15, aspartic acid molecule = 1, simulation box = 39.56 × 39.56 × 75.63 Å, forcefield: COMPASS, and simulation time = 200 ps.

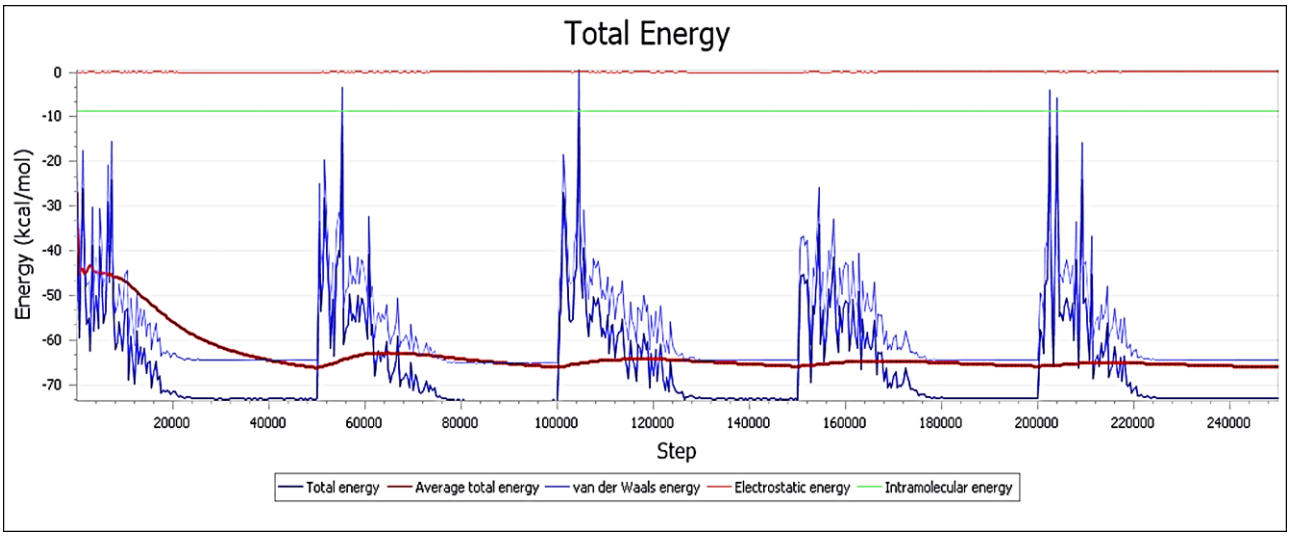

Figure 12: Total energy, average, van der Waals, electrostatic and intramolecular energy versus optimization steps

4. MODE OF ACTION

Figure 13 displays the mode of adsorption of aspartic acid on the mild steel. The adsorption isotherm, impedance, MM, and computational studies reveal the adsorption mechanism of aspartic acid on the MS. The aspartic acid forms a stable and uniform monolayer (LAI) on mild steel surface proved by the increase in R_{ct}, Warburg impedance, coating thickness, $E_{vibrational}$, thermal energy, ΔG°_{ads} and equilibrium adsorption constant (K_{ads}).[61] A strong donor-acceptor type bond was established between the carboxylic group of terminal acid and iron atoms of MS. The aspartic acid donates e^- to vacant d-orbital of MS and MS in anticipation donates its e^- to π* orbital of aspartic acid. The same was confirmed by significant electrochemical potential, global softness, and aspartic acid/mild steel interaction energy parameters.

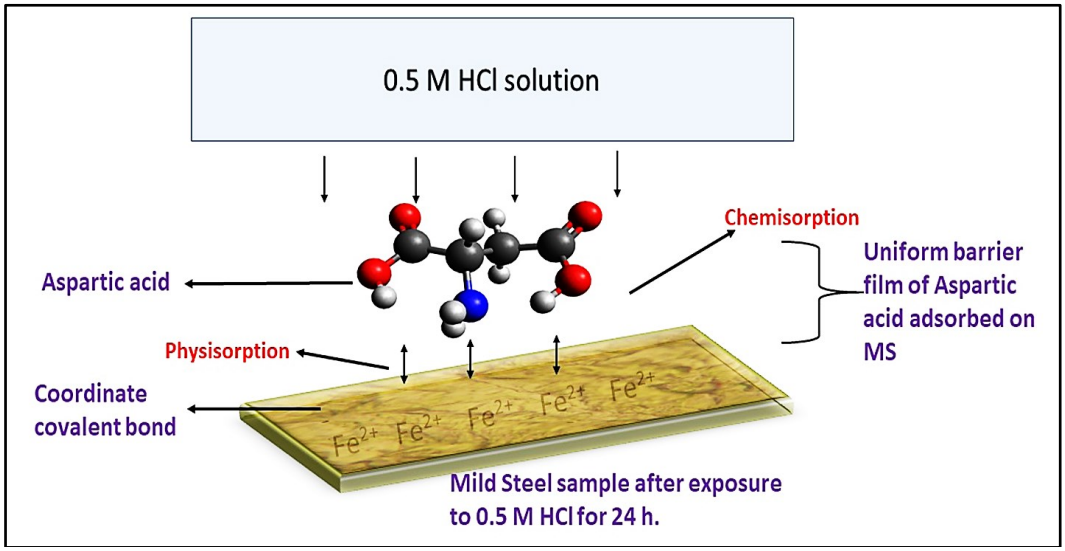

Figure 13: Mechanism of inhibition of Mulberry leaves extract for mild steel in 0.5 M HCl

5. BIOCOMPATIBILITIES OF ACID-TREATED WASTEWATER

"The maximum permissible limit of BOD and COD in H_2O is 30 and 250 mg/L. The BOD and COD was observed by Eqns. (21 and 22).[57]

BOD = DO of BB – DO of SB after 5 days. (21)

$$COD = \frac{8 \times 1000 \times DF_x M_x (V_B - V_S)}{Volume\ of\ sample\ taken} \quad (22)$$

Figure 14 shows results of biochemical testing of waste acid left after corrosion tests. The BOD/COD ratio of untreated acidified water provides information about biodegradability activity of the inhibitor molecule. Greater is the BOD/COD ratio, higher is the biodegradability of the molecule. If BOD/COD ratio lies between 0.24 - 0.36, then organic content present in it can be biodegradable easily.[42,43] The BOD and COD and their ratio in presence of 1000 ppm of aspartic acid were found within the permissible amount i.e., 24.7, 87.6, and 0.28 mg/L, respectively.

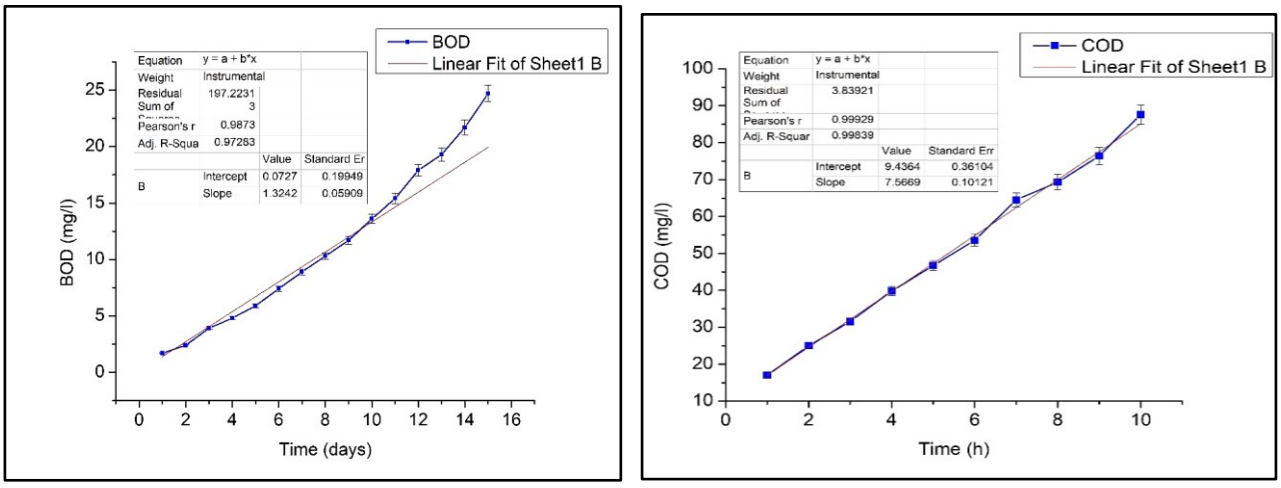

Figure 14: BOD and COD of acid left after gravimetric study after addition of 1000 ppm of Aspartic acid

6. CONCLUSIONS

Morus nigra (Mulberry leaves) was explored as a green CI for MS in 0.5 M HCl by experimental, surface, and theoretical methods. The surface study, thermodynamic and kinetic parameters were investigated by MM, LAI, FAI, and MDS techniques. The results obtained from the experimental study were supported by different theoretical (LAI and FAI) and computational (DFT, MDS, FMO) techniques. Spectroscopic characterization techniques like UV-visible, FTIR,

and NMR prove that aspartic acid was the major constituent present in Mulberry leaves extract which was responsible for the high inhibition efficiency shown by green inhibitor. The green inhibitor shows 91.62 % CIE at 1000 ppm concentration. The aspartic acid acts as a mixed CI as it affects both Tafel slopes. The Bode phase angle upsurges with an aspartic acid concentration in the medium. The R_{ct} and R_s upsurge with inhibitor concentration thus proving an increase in coating thickness with the concentration of green inhibitor. The surface roughness, pores, cracks, pits intensity decreases with green inhibitor concentration. The growth of insulating film increases with *Morus nigra* concentration. The theoretical and computational studies prove chemical and physical adsorption of aspartic acid on the MS. The chemical, thermodynamic and kinetic parameters i.e., global softness, electron-donation tendency, chemical potential, aspartic acid/MS interaction energy, and $E_{binding}$, and adsorption power confirm the presence of barrier film on the MS surface. The biochemical activity of unused acidified water was found in an acceptable limit.

Acknowledgements. *We author of this manuscript are grateful to the authorities of CUH for providing infrastructural support for this research work.*

Conflict of interest. *The authors declare that we have no financial or commercial Conflict of Interest.*

Data availability statement. *The data can be made available from the corresponding author upon written request.*

REFERENCES

1. J. I. Bhat, V. D. P. Alva. Inhibition effect of miconazole nitrate on the corrosion of mild steel in hydrochloric acid medium, *Intern. J. Electrochem*., **2011**, *2011*, Article ID 157576, 8 pages.
2. P. B. Raja, M. G. Sethuraman. Natural products as corrosion inhibitor for metals in corrosive media: A Review, *Mater. Lett*., **2008**, *62*, 2977-2979.
3. C. Jeyaprabha, S. Sathiyanarayanan, K. L. N. Phani, G. Venkatachari. Influence of poly(aminoquinone) on corrosion inhibition of iron in acid media, *Appl. Surf. Sci*., **2005**, *252*, 966-975.
4. M. A. Quraishi, A. Singh, V. K. Singh, D. K. Yadav, A. K. Singh. Green approach to corrosion inhibition of mild steel in hydrochloric acid and sulphuric acid solutions by the extract of *Murraya koenigii* leaves, *Mater. Chem. Phys*., **2010**, *122*, 114-122.
5. L. R. Chauhan, G. Gunasekaran. Corrosion inhibition of mild steel by plant extract in dilute HCl medium, *Corros. Sci*., **2007**, *49*, 1143-1161.
6. J. C. Rocha, J.A.C.P. Gomes, E. D'Elia. Corrosion inhibition of carbon steel in hydrochloric acid solution by fruit peel aqueous extracts, *Corros. Sci*., **2010**, *52*, 2341-2348.
7. A. Ostavari, S. M. Hoseinieh, M. Peikari, S. R. Shadizadeh, S. J. Hashemi. Corrosion inhibition of mild steel in 1 M HCl solution by henna extract: A comparative study of the inhibition by henna and its constituents (Lawsone, Gallic acid, α-d-Glucose, and Tannic acid), *Corros. Sci*., **2009**, *51*, 1935-1949.
8. P. C. Okafor, E. E. Ebenso. The inhibitive action of *Carica papaya* extracts on the corrosion of mild steel in acidic media and their adsorption characteristics, *Pigment & Resin. Tech*., **2007**, *36*, 134-140.
9. P. C. Okafor, M. E. Ikpi, I. E. Uwah, E. E. Ebenso, U. J. Ekpe, S. A. Umoren. Inhibitory action of *Phyllanthus amarus* extracts on the corrosion of mild steel in acidic media, *Corros. Sci*., **2008**, *50*, 2310-2317. https://doi.org/10.1016/j.corsci.2008.05.009
10. A. M. Abdel-Gaber, B. A. Abd-El-Nabey, M. Saadawy. The role of acid anion on the inhibition of the acidic corrosion of steel by lupine extract, *Corros. Sci*., **2009**, *51*, 1038-1042.
11. K. O. Orubite, N. C. Oforka. Inhibition of corrosion of mild steel in HCl solutions by the extracts of leaves of *Nypa fructicans* Wurmb, *Mat. Lett*., **2004**, *58*, 1768-1772.
12. V. V. Torres, R. S. Amado, C. F. de Sá, T.L. Fernandez, C.A.S. Riehl, A.G. Torres. Inhibitory action of aqueous coffee ground extracts on the corrosion of carbon steel in HCl solution, *Corros. Sci*. **2011**, *53*, 2385-2392.
13. L. G. Trindade, R. S. Goncalves. Evidence of caffeine adsorption on a low-carbon steel surface in ethanol, *Corros. Sci*., **2009**, *51*, 1578-1583.
14. A. Sharmila, A. A. Prema, P. A. Sahayaraj. Influence of *Murraya koenigi* (curry leaves) extract on the corrosion inhibition of carbon steel in HCl solution, *Rasayan J. Chem*., **2010**, *3(1*), 74-81.
15. S. A. Umoren, M. J. Banera, T. Alonso-Garcia, C. A. Gervasi, M. V. Mir´ıco. Inhibition of mild steel corrosion in HCl solution using chitosan, *Cellulose*, **2013**, *20*, 2529-2545.
16. S. A. Umoren, U. M. Eduok. Application of carbohydrate polymers as corrosion inhibitors for metal substrates in different media: A review, *Carbohydr. Polym*., 2016, *140*, 314-341.
17. S. A. Umoren, I. B. Obot, A. M. Kumar, Z. M. Gasem. Performance evaluation of pectin as ecofriendly corrosion inhibitor for X60 pipeline steel in acid medium: Experimental and theoretical approaches, *Carbohydr. Polym*., **2015**, *124*, 280-291.
18. H. Sashiwa, S. I. Aiba. Chemically modified chitin and chitosan as biomaterials, *Prog. Polym. Sci*., **2004**, *29*, 887-908.
19. A. Valbon, M. A. Neves, A. Echevarria. Anticorrosive effect of PVP 40000 against AISI 1020 carbon steel in HCl, *Mat. Res*., **2018**, *21.*
20. L. A. Juhaiman, A. A. Mustafa, W. K. Mekhamer. Polyvinyl pyrrolidone as a green corrosion inhibitor

of carbon steel in neutral solutions containing NaCl: Electrochemical and thermodynamic study, *Internat. J. Electrochem. Sci*., **2012**, *7*, 8578-8596.
21. L. A. Juhaiman. Polyvinyl pyrrolidone as a corrosion inhibitor for carbon steel in HCl, *Internat. J. Electrochem. Sci*., **2016**, *11*, 2247-2262.
22. N. Sainia, R. Kumar, P. Pahujaa, R. Malika, R. Malika, S. Singh, S. Lata. Exploring the capability of synthesized PVP-Oxime for corrosion inhibition of a mild steel surface in a 1 M H_2SO_4 solution, *Portu. Electrochimica Acta*, **2020**, *38*, 43-58.
23. A. R. Alkais, S. M. Edrah. The Corrosion inhibition of mild steel in acid solutions media by adsorption of leaves of *Morus nigra* L. from Libya, *Internat. J. Sci. Res*., **2016**, *5*, 730-734.
24. A. I. Ali, N. Foaud. Inhibition of aluminum corrosion in hydrochloric acid solution using black mulberry extract, *J. Mater. Environ. Sci*., **2012**, *3(5)*, 917-924.
25. Y. Qiang, S. Zhang, B. Tan, S. Chen, Evaluation of Ginkgo leaf extract as an eco-friendly corrosion inhibitor of X70 steel in HCl solution, *Corros. Sci*., **2018**, *133*, 6-16.
26. H. Li, Y. Qiang, W. Zhao, S. Zhang. 2-Mercaptobenzimidazole-inbuilt metal-organic-frameworks modified graphene oxide towards intelligent and excellent anti-corrosion coating, *Corros. Sci*., **2021**, *191*, 109715.
27. Q. Yujie, G. Lei, L. Hao, L. Xijian. Fabrication of environmentally friendly *Losartan potassium* film for corrosion inhibition of mild steel in HCl medium, *Chemical Engg. J*., **2021**, *406*, 126863.
28. K. K. Anupama, J. Abraham. Electroanalytical studies on the corrosion inhibition behavior of guava (*Psidium guajava*) leaves extract on mild steel in hydrochloric acid, *Res. Chem. Intermed*., **2013**, *39*, 4067-4080.
29. A. Thomas, M. Prajila, K. M. Shainy, A. Joseph. A green approach to corrosion inhibition of mild steel in hydrochloric acid using fruit rind extract of *Garcinia indica* (Binda), *J. Mol. Liq*., **2020**, *312*, 113369.
30. H. Kumar, D. Tilak. 5-Aminotetrazole a highly efficient corrosion inhibitor for mild steel in 0.1 M sulphuric acid: Experimental & theoretical study, *Chem. Data Collect*., **2021**, *33,* 100721.
31. H. Kumar, V. Yadav. Highly efficient and eco-friendly acid corrosion inhibitor for mild steel: Experimental and theoretical study, *J. Mol. Liq*., **2021**, *116220*.
32. H. Kumar, D. Tilak. Cyclohexylamine an effective corrosion inhibitor for mild steel in 0.1 N H_2SO_4: Experimental and theoretical (Molecular dynamics simulation and FMO) the study, *J. Mol. Liq*., **2020,** *32*, 114847.
33. H. Kumar, S. Yadav, R. S. Chaudhary, D. Kumar. Synergistic effect of some antiscalants as Corrosion inhibitor for Industrial Cooling Water System, *J. Appl. Electrochem*., **2009**, *39*, 1339-1347.
34. H. Kumar, D. Tilak. Cetyl trimethyl ammonium bromide as anti-pit agent for mild steel in sulfuric acid medium, *Current Phys. Chem.*, **2020**, *10*, 1-14.
35. S. Ghareba, S. Omanovic. Interaction of 12-aminododecanoic acid with a carbon steel surface: Towards the development of 'green' corrosion inhibitors, *Corros. Sci*., **2010**, *52*, 2104-2113.
36. C. Jeyaprabha, S. Sathiyanarayanan, K. L. N. Phani, G. Venkatachari. Influence of poly(aminoquinone) on corrosion inhibition of iron in acid media, Appl. Surf. Sci., **2005**, *252*, 966-975.
37. M. J. Frisch, G. W. Trucks, H. B. Schlegel, G. E. Scuseria, M. A. Robb, J. R. Cheeseman, G. Scalmani, V. Barone, B. Mennucci, G. A. Petersson, H. Nakatsuji, M. Caricato, X. Li, H. P. Hratchian, A. F. Izmaylov, J. Bloino, G. Zheng, J. L. Sonnenberg, M. Hada, M. Ehara, K. Toyota, R. Fukuda, J. Hasegawa, M. Ishida, T. Nakajima, Y. Honda, O. Kitao, H. Nakai, T. Vreven, J.A. Montgomery, Jr., J. E. Peralta, F. Ogliaro, M. Bearpark, J. J. Heyd, E. Brothers, K. N. Kudin, V. N. Staroverov, R. Kobayashi, J. Normand, K. Raghavachari, A. Rendell, J. C. Burant, S. S. Iyengar, J. Tomasi, M. Cossi, N. Rega, J. M. Millam, M. Klene, J.E. Knox, J. B. Cross, V. Bakken, C. Adamo, J. Jaramillo, R. Gomperts, R. E. Stratmann, O. Yazyev, A. J. Austin, R. Cammi, C. Pomelli, J. W. Ochterski, R. L. Martin, K. Morokuma, V. G. Zakrzewski, G. A. Voth, P. Salvador, J. J. Dannenberg, S. Dapprich, A. D. Daniels, Ö. Farkas, J. B. Foresman, J. V. Ortiz, J. Cioslowski, D. J. Fox. Gaussian, Inc., Wallingford CT, **2009**.
38. Z. Cao, Y. Tang, H. Cang, J. Xu, G. Lu, W. Jing. Novel benzimidazole derivatives as corrosion inhibitors of mild steel in the acidic media. Part II: theoretical studies, *Corros. Sci*., **2014**, *83,* 292-298.
39. J. A. Ciezak, S. F. Trevino. Inelastic neutron scattering spectrum of cyclotrimethylene trinitramine: A comparison with solid-state electronic structure calculations, *J. Phys. Chem. A*., **2006**, *110*, 5149-5155.
40. L. Pauling. *The Nature of the Chemical Bond*, Cornell University Press, New York, **1960**.
41. S. K. Saha, P. Ghosh, A. Hens, N. C. Murmu, P. Banerjee. Density functional theory and molecular dynamics simulation study on corrosion inhibition performance of mild steel by mercapto-quinoline Schiff base corrosion inhibitor, *Physica E*., **2015**, *66*, 332-341.
42. J. S´anchez-Mart´ın, J. Beltr´an-Heredia, C. Solera Hern´andez. Surface water and wastewater treatment using a new tannin-based coagulant, Pilot plant trials, *J. Environ. Manage*., **2010**, *91*, 2051-2058.
43. L. Huang, S. Cheng, F. Rezaei, B. E. Logan. Reducing organic loads in wastewater effluents from paper recycling plants using microbial fuel cells, *Environ. Technol*., **2009**, *30*, 499-504.
44. D. S. Mahesh, B. S. Vidhathri, D. N. Vidyashree, T. K. Narayanaswamy, C. T. Subbarayappa, R. Muthuraju. Biochemical Composition and Pharmacological Properties of Mulberry (*Morus* spp.)

- A Review, *Int. J. Curr. Microbiol. App. Sci*., **2017**, *6(7)*, 2207-2217.
45. R. Chadli, M. Elazouzi, I. Khelladi, A.M. Elhourri, H. Elmsellem, A. Aouniti, J. Kajima Mulengi, B. Hammouti. Electrochemical and theoretical study of pyrazole 4-(4,5-dihydro-1*H*-pyrazol-5-yl)-N,N-dimethylaniline (D) as a corrosion inhibitor for mild steel in 1 M HCl, *Portugaliae Electrochimica Acta*, **2017**, *35(2)*, 65-80.
46. K. Rajan, S. Rajendran, R. Saranya. *Alium sativum* (garlic) extract as nontoxic Corrosion inhibitor, *J. Chem*., **2013**, *743807*, 1-4.
47. M. El Azzouzi, A. Aouniti, S. Tighadouin, H. Elmsellem, S. Radi, B. Hammouti, A. El Assyry, F. Bentiss, A. Zarrouk. Some hydrazine derivatives as corrosion inhibitors for mild steel in 1.0 M HCl: weight loss, electrochemical, SEM and theoretical studies, *J. Mol. Liq*., **2016**, *221*, 633-641.
48. Mohammad Mobin, Marziya Rizvi. Polysaccharide from Plantago as a green corrosion inhibitor for carbon steel in 1 M HCl solution, *Carbohydr. Polym*. **2017**, *160*, 172-183.
49. D. K. Yadav, M. Quraishi. Electrochemical investigation of substituted pyranopyrazoles adsorption on mild steel in acid solution, *Ind. Eng. Chem. Res*., **2012**, *51*, 8194-8210.
50. C. Verma, M. Quraishi, A. Singh. 2-Amino-5-nitro-4, 6-diarylcyclohex-1-ene-1,3,3-tricarbonitriles as new and effective corrosion inhibitors for mild steel in 1 M HCl: Experimental and theoretical studies, *J. Mol. Liq*., **2015**, *212*, 804-812.
51. A. S. Fouda, M. A. Ismail, G. Y. Elewady, A. S. Abousalem. Evaluation of 4-aminophenyl-2,2′-bithiophene and its aza-analog as novel corrosion inhibitors for CS in acidic media: Experimental and theoretical study, *J. Mol. Liq*., **2017**, *240*, 372-388.
52. M. Yadav, S. Kumar, N. Tiwari, I. Bahadur, E. E. Ebenso. Experimental and quantum chemical studies of synthesized triazine derivatives as an efficient corrosion inhibitor for N80 steel in acidic medium, *J. Mol. Liq*., **2015**, *212*, 151-167.
53. R. A. Alberty, R. J. Silbey. *Physical Chemistry*, Wiley, **1997**.
54. E. B. Barmatov, J. F. Gedded, L. P. Crawford, T.L. Hughes, N. V. Michaela. *US patent application no. 15/533, 315*, **2017**.
55. D. Daoud, T. Doudi, H. Hamani, S. Chafaa, M. Al Noaimi. Corrosion inhibition of mild steel by two new S-heterocyclic compounds in 1 M HCl: Experimental and computational study, *Corros. Sci*., **2015**, *94*, 21-37.
56. I. B. Obot, Z. M. Gasem, S. A. Umoren. Molecular-level understanding of the mechanism of aloes leaves extract inhibition of low carbon steel corrosion: a DFT approach, *Int. J. Electrochem. Sci*., **2014**, *9*, 510-522.
57. A. Kokalj. Is the analysis of the molecular electronic structure of corrosion inhibitors sufficient to predict the trend of their inhibition performance, *Electrochim. Acta*., **2010**, *56*, 745-755.
58. N. Kovacevic, A. Kokalj. Analysis of the molecular electronic structure of imidazole and benzimidazole-based inhibitors: a simple recipe for qualitative estimation of chemical hardness, *Corros. Sci*., **2011**, *53*, 909-921.
59. S. Erdoğan, Z. S. Safi, S. Kaya, D. O. Isin, L. Guo, C. Kaya. A Computational study on corrosion inhibition performances of novel quinoline derivatives against the corrosion of iron, *J. Mol. Struct*., **2017**, *1134*, 751.
60. S. A. Paul, S. K. Chavan, S. D. Khambe. Studies on the characterization of textile industrial wastewater in Solapur city, *Int. J. Chem*., **2012**, *10*, 635-642.
61. L. Li, S. Zhang, G. Li, H. Zhao. Determination of chemical oxygen demand of nitrogenous organic compounds in wastewater using synergetic photo-electrocatalytic oxidation effect at TiO_2 nanostructured electrode, *Anal. Chim. Acta*., **2012**, *754*, 47-53.

Corresponding author: **Harish Kumar**
Department of Chemistry, Central University of Haryana
Mahendergarh, 123 031, India
E-mail: harishkumar@cuh.ac.in.